Journal of ELECTRONIC MATERIALS, Vol. 45, No. 2, 2016
DOI: 10.1007/s11664-015-4235-1

Structural, Optical and Electrical Characteristics of a $La_{0.5}K_{0.5}Ga_{0.5}V_{0.5}O_3$ System

TRUPTIMAYEE ACHARYA[1,2] and R.N.P. CHOUDHARY[1]

1.—Department of Physics, Institute of Technical Education & Research, Siksha 'O' Anusandhan University, Khandagiri, Bhubaneswar 751030, Odisha, India. 2.—e-mail: truptiacharya18@gmail.com

The polycrystalline sample of $La_{0.5}K_{0.5}Ga_{0.5}V_{0.5}O_3$ (LKGVO) was prepared using a high-temperature solid-state reaction technique. X-ray structural analysis of the sample confirmed the formation of a single-phase compound in an orthorhombic crystal system. Preliminary molecular structural analysis using infrared (IR) spectroscopy further supports the formation of a single-phase compound. The optical indirect band gaps in LKGVO were obtained from the ultraviolet–visible light (UV–Vis) absorption spectral analysis. The micro-structural study on the LKGVO pellet sample by scanning electron microscopy shows that well-defined grains are distributed uniformly throughout the surface of the sample. Detailed studies of dielectric and impedance parameters as a function of temperature and frequency have shown the significant effect of grains and grain boundaries in the relaxation process. A *I–V* characteristic of the material shows a negative temperature co-efficient of resistance which is similar to that of a semi-conductor. Based on the appearance of a distinct dielectric anomaly and an unsaturated *P–E* hysteresis loop, like many other compounds, the existence of ferroelectricity in the compound can be expected in spite of it having moderate ionic conductivity.

Key words: X-ray diffraction, infrared spectroscopy, dielectric properties, conductivity, ferroelectricity

INTRODUCTION

Nowadays, a large number of materials of different structural families are available for solid-state devices. Among them, some oxides of the ABO_3 (A = mono-divalent, B = tri-penta valent ions) family are widely used for multifunctional devices such as sensors, memory devices, detectors, solid oxide fuel cells (SOFCs), oxygen pumps, etc. It is interesting to observe simultaneously insulating (ferroelectric) as well as conducting (ferrite) characteristics in some of them, such as bismuth ferrite, lanthanum gallate, etc. Lanthanum gallate ($LaGaO_3$; with some modification) has been found to be a promising material which can be used for various purposes: (i) as an electrolyte material of SOFCs,[1] (ii) as a substrate material for superconducting film,[2] (iii) as a high dielectric-k material,[3] etc. It has a distorted perovskite-type (orthorhombic) structure with a phase transition at 150°C.[4] In order to develop materials for the above devices, compositional modifications or/and formation of a composite have been found useful. Therefore, in the search for a new material for possible multifunctional devices, several attempts have been made to modify the composition of $LaGaO_3$ with different types and amounts of substituents at its different atomic sites. Ishihara et al. suggested[5] that high ionic conductivity in this material can be induced by introducing an oxide-ion vacancy with partial substitution of Sr^{2+} at the La^{3+} site and Mg^{2+} at the Ga^{3+} site. Doping a small amount of Sr at the La site and Mg and Co at the Ga site of $LaGaO_3$ has been found to be effective for increasing the ionic conductivity of the oxide.[6,7] Raghavender et al.[8] found that Ba-, Sr- and Mg-doping in $LaGaO_3$ is more effective for this purpose. On partial substitution, not only the conducting property, but also the phase

(Received June 20, 2015; accepted November 7, 2015; published online December 8, 2015)

transition behavior of the material, can be controlled. From the detailed literature survey, it is found that not much attention has been paid on the studies of the effect of structural defects on the optical and electrical properties (including ionic conductivity) of a solid solution of ferroelectric and ionic insulators (KVO_3 and $LaGaO_3$) in equal ratios [i.e., $La_{0.5}K_{0.5}Ga_{0.5}V_{0.5}O_3$ (LKGVO)]. Therefore, we propose to study the structural, optical and electrical characteristics of the solid solution (LKGVO) at and above room temperature and at atmospheric pressure. It is expected that the replacement of La of $LaGaO_3$ by K ions of KVO_3 may help to (i) stabilize the crystal structure, and (ii) create oxygen vacancies. These situations can be utilized to achieve ferroelectricity as well as ionic conductivity in LKGVO.[9]

EXPERIMENTAL DETAILS

The polycrystalline sample of $La_{0.5}K_{0.5}Ga_{0.5}V_{0.5}O_3$ (LKGVO) was prepared using high-purity La_2O_3 (99.9%, M/s Loba Chemie), Ga_2O_3 (99.999%, M/s Loba Chemie), K_2CO_3 (99.9%, M/s Loba Chemie), and V_2O_5 (99.9%) by a three-step synthesis method; (i) mechanical mixing (both dry mixing and wet mixing), (ii) high-temperature calcinations in an air atmosphere at 1250°C for 4 h and (iii) high-temperature sintering at 1300°C for 4 h in an air atmosphere. The formation and quality of the material were checked at every step using an x-ray diffraction (XRD) technique. For structural analysis, the XRD pattern was obtained in a wide range of Bragg angles 2θ ($20° \le 2\theta \le 80°$) with a λ wavelength = 1.5405 Å ($Cu_{K\alpha}$ radiation) using an x-ray powder diffractometer (model D8 Advance, Bruker Corporation). Study of scanning electron micrographs of the pellet sample of LKGVO (with a thickness of 10 mm and area of 73 mm^2) at room temperature depicts the surface morphology (i.e., grain size, distribution, voids, etc.) of the sample. For dielectric and electrical characterizations, both of the parallel surfaces of the pellets were coated with high-quality silver paint. The dielectric constant, tangent loss, impedance, and phase angle of LKGVO were obtained as a function of frequency (1 kHz – 1 MHz) at different temperatures (25–450°C) using a phase sensitive meter (PSM 1735, N4L). *I-V* characteristics of the sample were measured at the interval of 25°C from room temperature to 450°C using a programmable electrometer (Keithley, model 6517B). The hysteresis loop of the poled sample was traced using a *P–E* hysteresis loop tracer (version 4.9.0 of Radiant Technologies, Inc.). The Fourier transform infrared (FTIR) spectra were recorded in a KBr medium between 4000 cm^{-1} and 400 cm^{-1} using a JASCO FT/IR-4100 spectrometer. The UV–Vis spectra were recorded using a JASCO V-630 spectrometer.

RESULTS AND DISCUSSION

Structural and Micro-Structural Analysis

The room-temperature XRD pattern (Fig. 1a) of the calcined powder of LKGVO shows the formation of a single-phase compound. All the peaks of the pattern were indexed in different crystal systems and unit cell configurations. Based on the minimum value of difference in the observed and calculated inter-planar spacing, an orthorhombic crystal system was selected. The lattice parameters of the selected unit cell were refined using the least-squares sub-routine of the standard computer program "PowdMult".[10] The least-squares refined unit cell parameters are: a = 18.799 Å, b = 16.529 Å, c = 6.077 Å and V = 1888.3 $(A^0)^3$ (with an estimated standard deviation of the unit cell parameters = 0.004 Å). Though these values of LKGVO are different from those of its component materials ($LaGaO_3$ and KVO_3), they are related to and consistent with those of their component oxides. The crystallite size (P) of LKGVO was estimated from the peak broadening $\beta_{1/2}$ (peak width at half-height) and position (2θ) of some higher angle reflections using Scherrer's relation,[11] $P = k\lambda/\beta_{1/2}\cos\theta$ (k = constant = 0.89, λ = 0.15407 nm). The value of the crystallite size was found to be ≅44 nm. The broadening due to strain, instruments and others factors was ignored in the calculation of P because of the use of the powder sample for the XRD pattern. The tolerance factor, t, which depicts geometric packing within a perovskite structure, is defined by the equation,[12]

$$t = \frac{(r_A + r_O)}{\sqrt{2}(r_B + r_O)} \quad (1)$$

where r_A, r_B and r_O are the average ionic radii of the A-site cation, B-site cation and anion, respectively. The estimated value of t was found to be 0.91. The deviation in the value of t from that of the stable perovskite structure (t = 1) clearly exhibits distortion of the perovskite structure to form a new crystal system with different cell parameters.

The scanning electron micrograph of the surface of gold-sputtered, sintered pellet sample is shown in Fig. 1b (inset). The micrograph generally exhibits platelet-shaped dense grains that are randomly but uniformly distributed and oriented. The grain size of the sample is within a range of 3–10 μm. Furthermore, the micrograph indicates the polycrystalline texture of the compound. Though the presence of some pores/voids in the microstructure affects the conductivity and other related parameters, LKGVO still has reasonably high ionic conductivity which can be used in fabrication of an electrolyte for SOFCs.

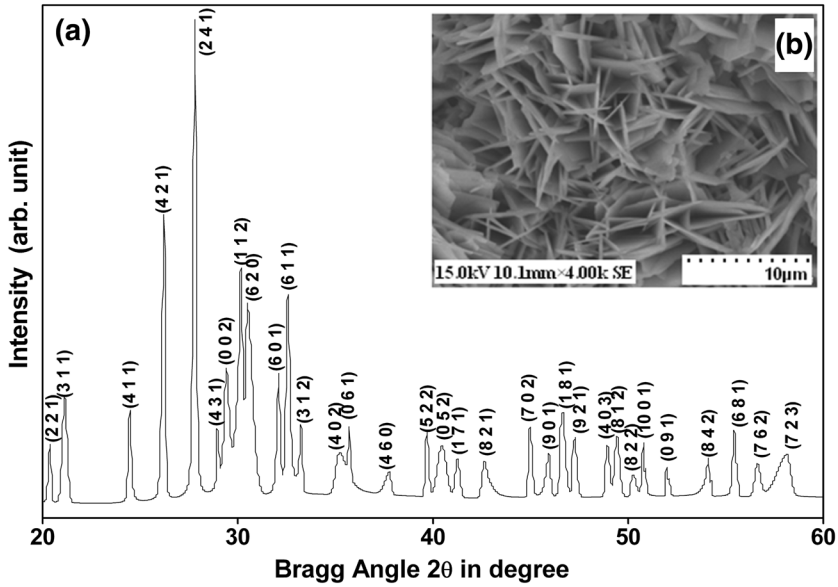

Fig. 1. (a) X-ray diffraction pattern of $La_{0.5}K_{0.5}Ga_{0.5}V_{0.5}O_3$, (b) SEM micrograph of $La_{0.5}K_{0.5}Ga_{0.5}V_{0.5}O_3$.

Infrared Spectral Analysis

As infrared (IR) spectroscopy gives information about the chemical composition and molecular structure of the materials, the FTIR spectra of LKGVO was recorded with a wide range of wave numbers (4000–400 cm^{-1}) at room temperature (Fig. 2a). Generally, the La-O asymmetric stretching band is observed at 514 cm^{-1},[13] but upon substitution of the K^+ ion at the La-site, the band shifts to the lower frequency. Thus, taking the band shifting into account, we attribute the mode located at 495 cm^{-1} of the FTIR spectrum to an La-O asymmetric stretching band. Again, Nadi[14] ascribed the band at 970 cm^{-1} as La–O stretching vibrations. Because of the substitution of a K^+ ion at the La-site in LKGVO, the band shifts to a slightly lower frequency; hence, the band at 964 cm^{-1} is assigned to La-O stretching vibration. The bands corresponding to the Ga-O stretching modes were observed at 811 cm^{-1} and 688 cm^{-1}.[15,16] The band at 431 cm^{-1} is assigned to the O-Ga-O bending mode vibration, which are in accordance with the earlier reports.[15] The IR spectra of pure V_2O_5 exhibits symmetric stretching modes of the V-O-V bonds at 826 cm^{-1}.[17] In comparison to V_2O_5 , the V–O vibrational frequency mode in LKGVO shifts towards a lower frequency, and, hence, the symmetric stretching bands of the V-O-V bonds are observed at 811 cm^{-1}.The IR band at 1023 cm^{-1} is attributed to a stretching mode (V=O).[17]

Ultraviolet–Visible Light Absorption Spectroscopy Analyses

The optical absorbance spectra of LKGVO powder are presented in Fig. 2b. The optical band gap energy (E_g) was estimated by the Wood and Tauc relation.[18] According to the following relation, the optical band gap is associated with absorbance and photon energy may be estimated:

$$h\upsilon\alpha \propto \left(h\upsilon - E_g\right)^k \tag{2}$$

where α is the absorbance, h is Planck's constant, υ is the frequency, E_g is the optical band gap and k is a constant whose value depends on the nature of the band transitions. For different transitions, the value of k was estimated to be 0.5, 2, 1.5 and 3 for direct allowed, indirect allowed, direct forbidden and indirect forbidden bands, respectively.[19] The band gap of LKGVO powder was evaluated from the Tauc plot by extrapolating from the linear portion of the graph (as shown in Fig. 2b). The value of the indirect band gap for LKGVO came out to be 4.59 eV. The indirect band gap value of $LaGaO_3$ was reported to be 4.22 eV[20] and 4.4 eV[21] from experimental analysis which is consistent with the calculated value (3.74 eV).[21] The band gap of KVO_3 was reported to be within 4–4.5 eV.[22] Thus, the band gap of LKGVO is found to be increased from its reactants $LaGaO_3$ and KVO_3.

Dielectric Properties

Figure 3a shows the frequency dependence of the dielectric constant (ε_r) and loss tangent ($\tan\delta$) of LKGVO at different temperatures (150–400°C). The values of the dielectric constants are found to be very high at low frequencies (ε_r = 124,077 at 400°C). In the low-frequency region, the dielectric constant decreases strongly, whereas it decreases quite slowly in the high-frequency region. This type of dielectric behavior of the material can be explained by the Maxwell–Wagner and Koop's phenomenological models.[23] According to these models, the

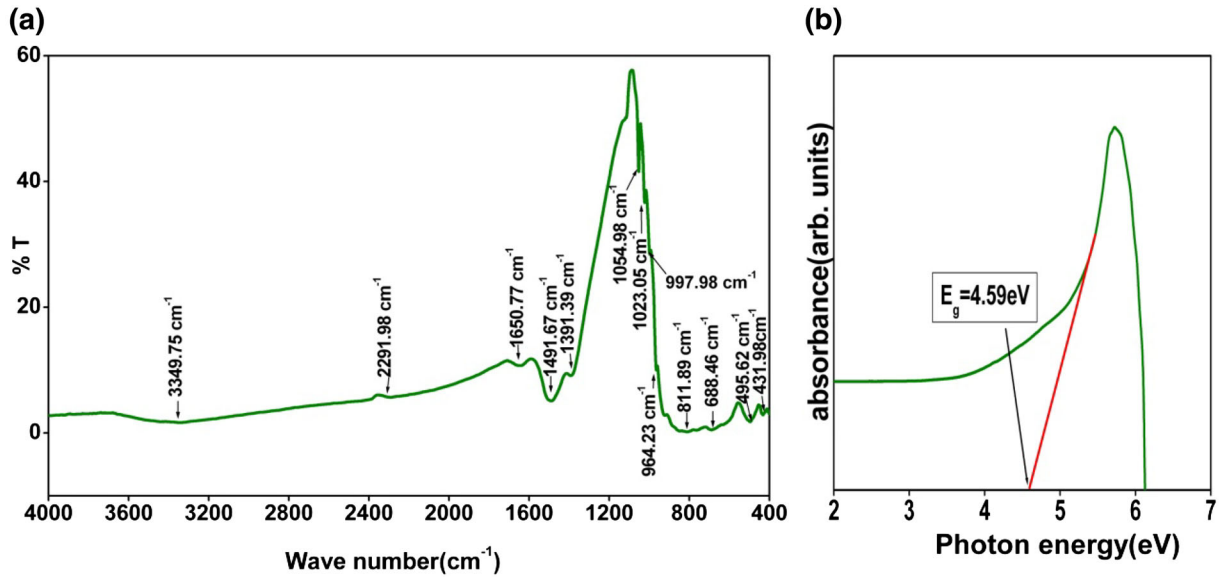

Fig. 2. (a) FTIR spectra of $La_{0.5}K_{0.5}Ga_{0.5}V_{0.5}O_3$, (b) UV spectra of $La_{0.5}K_{0.5}Ga_{0.5}V_{0.5}O_3$.

dielectric structure of the ceramic material is made up of two layers; one layer has highly conductive grains, whereas the other has poorly conducting grain boundaries. The grains are found to be more effective at higher frequencies, while at lower frequencies, the grain boundaries are more effective. The dielectric constant has a larger value in the low-frequency region, which may be attributed to large space charge polarization due to accumulation of electrons at poorly conducting grain boundaries, which play a dominant role in this frequency range. The movement of electrons inside the dielectric materials at higher frequencies is hindered because of the rapid change in their direction of motion, which may be one of the reasons for decreasing values of ε_r with frequency.[24] The electron transfer between the states Ga^{3+} to Ga^{2+} (depending on oxygen stoichiometry) can lead to an increase in conductivity,[25] and, thus, the ceramic sample shows relatively high dielectric properties. But in LKGVO, the electron hopping between Ga^{3+} to Ga^{2+} cannot follow the high-frequency ac field and it may be responsible for the decreasing trend of ε_r with an increase in frequency.

Figure 3b shows the variation of the tangent loss ($\tan\delta$) with frequency. In the $\tan\delta$–frequency plot, well-defined peaks are observed and, with an increase in temperature these peaks are shifting to higher frequencies. The shifting of the loss peaks with temperature suggests the dielectric relaxation phenomena is occurring in the material.[26]

The temperature dependence of the relative dielectric constant (ε_r) and tangent loss ($\tan\delta$) at different frequencies (1 kHz, 10 kHz, 100 kHz, 500 kHz and 1000 kHz) is shown in Fig. 3c and d, respectively. It was observed from the plots that the value of dielectric constant is almost constant in the low- and medium-temperature ranges (i.e., up to 200°C), and then it gradually increases with increasing temperature up to its maximum value (ε_{max}) at the Curie temperature (T_c) and then decreases with a further increase in temperature. As LKGVO is the combination of two ferroelectric materials, $LaGaO_3$ and KVO_3 have well-defined transition temperatures at ~145°C[27] and 322°C[28], respectively. A resultant dielectric anomaly of a new combined system (LKGVO) is expected within a range of 145–322°C. A little deviation from our expected peak was observed at 335°C in the present dielectric study. This dielectric anomaly is assumed to be related to the ferroelectric–paraelectric phase transition, and the appearance of a hysteresis loop at room temperature (below T_c) confirmed this assumption. Another very weak, diffused dielectric anomaly is observed at 249°C. This dielectric anomaly does not correspond to ferroelectric phase transitions. It may be related to the change in conductivity. Above T_c, the decrease in ε_r indicates the paraelectric behavior of the LKGVO samples. However, above 375°C, the increase in ε_r can be understood in terms of a thermally activated transport property and the presence of space charges. As the sintering temperature of LKGVO is very high, the contribution of space charge in the dielectric constant may be due to oxygen vacancies (OVs). As LKGVO shows the frequency dependence of the transition temperature, it suggests the existence of a relaxation process in the material. Figure 3d shows variation of $\tan\delta$ with temperature which follows a pattern similar to ε_r. In the low-temperature region, the rate of $\tan\delta$ increase is found to be small, whereas at higher temperatures, it increases significantly. The generation of a large number of charge carriers and defects in the sample leads to a

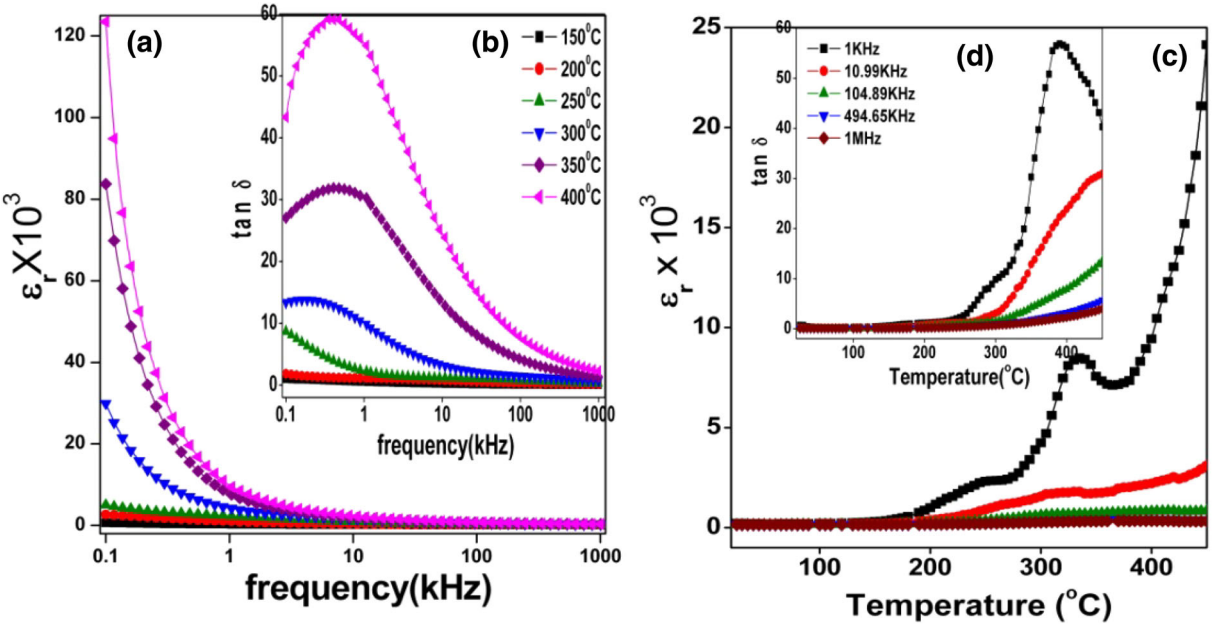

Fig. 3. Variation of (a) relative dielectric constant (ε_r) and (b) tangent loss (tan ð; in inset) with frequency at different temperatures. Variation of (c) relative to dielectric constant (ε_r) and (d) tangent loss (tan ð; in inset) with temperature at different frequencies of $La_{0.5}K_{0.5}Ga_{0.5}V_{0.5}O_3$.

rise in conductivity and this may be responsible for the sharp increase in tanδ at higher temperatures. Moreover, the contribution of ferroelectric domain walls to tanδ being less causes the rise in tanδ values at high temperatures.[29] The decrease of the maximum value of relative dielectric constant and tangent loss (ε_{max} and tanδ_{max}) with frequency, as observed from Fig. 3c and d, is a normal trend in ferroelectric materials. The loss of oxygen during high-temperatures sintering leads to ionic conductivity, which may be attributed to the dispersion of tanδ at a higher temperature. In the region of phase transition the dielectric peaks were found to be broadened. The degree of disorder or diffusivity of the peaks can be estimated by calculating the diffusivity (γ) using the empirical relation,[30]

$$\frac{1}{\varepsilon_r} - \frac{1}{\varepsilon_{max}} = \gamma \ln(T - T_c) + \text{constant} \qquad (3)$$

where ε_r, ε_{max} are the relative dielectric constant and its maximum value at temperature T and T_c , respectively. The type of phase transition can be determined from the value of γ. For materials obeying the normal Curie–Weiss law, $\gamma = 1$, whereas for a completely disordered system, its value is 2. From Fig. 4b, the diffusivity (γ) was found to be 1.8 at 1 kHz and this confirms the diffuse phase transition of LKGVO.

As LKGVO was sintered at a very high temperature, there may be oxygen vacancy at such a high sintering temperature and this can be represented by using Kröger and Vink notation[31] as:

$$O_o \rightarrow 1/2O^2 \uparrow + V_0'' + 2e^- \qquad (4)$$

where V_0'' denotes oxygen vacancies. The defects such as oxygen vacancies (V_0'') induce disorder in the system,[32] and, thus, the diffuse type phase transition occurs.

Polarization Study

Figure 4a shows the hysteresis loop of the LKGVO ceramic measured at various electric fields at room temperature at 200 Hz. The ferroelectricity of the material at room temperature is confirmed by the occurrence of a polarization–electric field hysteresis loop at that temperature. From the hysteresis loop, it is seen that the polarization ($2P_r$) and coercive fields ($2E_C$) increase with an increased electric field. The remnant polarization ($2P_r$) and coercive field ($2E_C$) measured at 6 kV (200 Hz) are found to be 0.48 μC/cm^2 and 38.7 kV/cm, respectively, and at 7 kV (200 Hz), these parameters are found to be 0.58 μC/cm^2 and 45.9 kV/cm, respectively. However, the value of the saturation polarizations ($2P_s$) measured at 6 kV and 7 kV are found to be 0.44 μC/cm^2 and 0.52 μC/cm^2, respectively. The remnant polarization in both loops is marginally more than that of saturation polarization. The reasons behind this may be (i) induced polarization, (ii) non-uniform polarization because of a polarization gradient, (iii) inhomogeneous domains created in/on the surface of sample, and/or (iv) influence of the electrode at a microscopic level. From the dielectric data, we obtained the transition

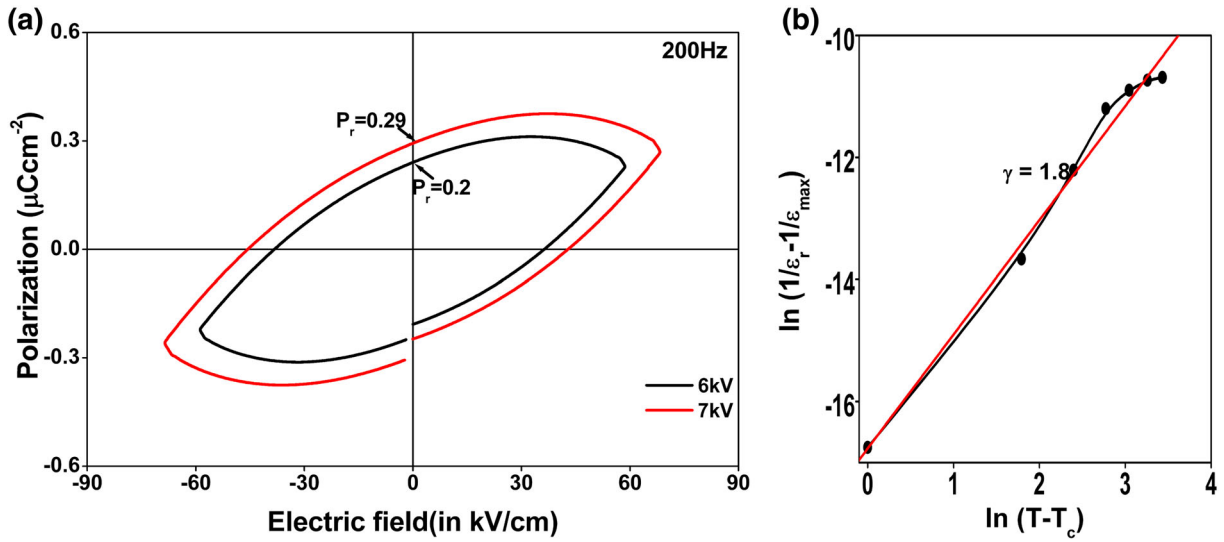

Fig. 4. (a) P–E hysteresis loop for various fields at room temperature of $La_{0.5}K_{0.5}Ga_{0.5}V_{0.5}O_3$, (b) Variation of ln $(1/\varepsilon_r - 1/\varepsilon_{max})$ with ln $(T - T_c)$ of $La_{0.5}K_{0.5}Ga_{0.5}V_{0.5}O_3$.

temperature at 335°C. It was not possible to check the transition temperature (obtained with dielectric study) due to limited experimental temperature facilities. The nature of the loop clearly suggests that the lack of a sufficient electric field, the existence of a high leakage current, a high tangent loss and the high ionic conductivity of the material have prevented a saturated hysteresis loop to confirm proper ferroelectricity in the sample. However, the observation of ferroelectricity in LKGVO is very much consistent with others where this property (ferroelectricity) has been reported in many oxide ionic conductors of a different structural family, namely, $Na_{1/2}Bi_{1/2}TiO_3$,[33] $Bi_5TiNbWO_{15}$,[34] $Ca_9Bi(VO_4)_7$,[35] $Ba_5Li_2Ti_2Nb_8O_{30}$,[36] $Ba_3(TiNb_4)0_{15}$,[37] $K_6Li_4Ta_{10}O_{30}$–$Pb_5Ta_{10}O_{30}$.[38] Further, based on the dielectric anomaly and an even unsaturated hysteresis loss, one may accept the existence of ferroelectricity in LKGVO. However, some more experiments can help support the above finding of the materials.

Impedance Spectroscopy

The impedance data recorded over a wide frequency range at various temperatures is shown as a Nyquist diagram in Fig. 5. The plots are analyzed by distorted or depressed semicircles, whose centers lie below the real axis. This decentralization follows Cole–Cole's formalism:

$$Z^*(\omega) = R/\left[1 + (j\omega/\omega_o)^{1-n}\right] \quad (5)$$

The depressed semicircle designates a non-Debye type of relaxation, i.e., a phenomenon with a distribution of relaxation times. The value of n is in between zero and one. This exponential parameter shows the distribution of relaxation times.[39,40] The non-ideal or non-Debye behavior is correlated to several factors as the grain size distribution, grain orientation, grain boundaries, etc. The appearance of single semicircular arcs at 150°C in the Nyquist plots stipulates that electrical conduction is owing to the bulk effect only, which is well-fitted by a parallel R–C circuit. The occurrence of double semicircular arcs at 200°C and 250°C manifests that electrical conduction is owing to the bulk and grain boundary effects, and modeled by a series combination of two parallel R–C circuits. As three semicircular arcs are observed within the temperature range of 280–450°C, electrical conduction in this temperature range owes not only to the bulk and grain boundary effect but also to the electrode polarization, which is well fitted by a series combination of three parallel R–C circuits.[41] The intercept of the semicircular arc on the real axis (Z') gives values of bulk resistance (R_b), grain boundary resistance (R_{gb}) and electrode resistance (R_e) at different temperatures, which are given in Table I. From the table, it can be noted that the values of R_b, R_{gb} and R_e decrease with an increase in temperature, which points out the reduction in resistive behavior of the material.

The frequency dependence of Z' and Z'' at selected temperatures is shown in Fig. 6a and b within the frequency range of 100 Hz to 1 MHz. The value of Z' decreases with a rise in both the frequency and temperature, which indicates an increase in its conductivity. The decrease in the magnitude of Z' with increasing temperature in the low-frequency region shows the negative temperature coefficient of resistance (NTCR) behavior of the material. The release of space charges may be responsible for the merger of curves[42] at a high frequency, and this, in turn, results in the lowering of the barrier properties of LKGVO in that frequency at higher temperatures.

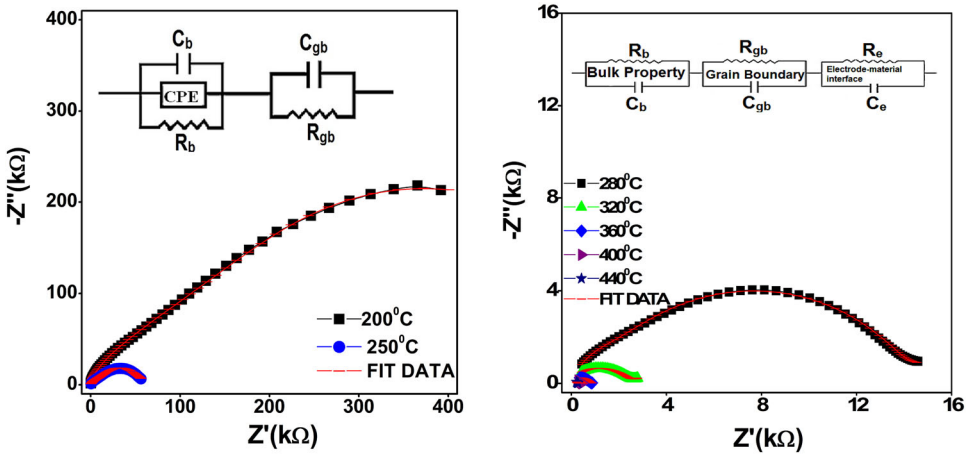

Fig. 5. Variation of Z′ with Z″ of $La_{0.5}K_{0.5}Ga_{0.5}V_{0.5}O_3$ at different temperatures.

Table I. Comparison of bulk resistances (R_b), grain boundary resistances (R_{gb}), electrode resistances (R_e), n values and dc conductivities (from Nyquist plots and conductivity measurements) at various temperatures

Temperature (in °C)	R_b (in Ω cm^2)	R_{gb} (in Ω cm^2)	R_e (in Ω cm^2)	N	σ_{DC} (S cm^{-1})	σ_{DC} (S cm^{-1})
100	6.57×10^7	–	–	0.68	2.76×10^{-7}	2.35×10^{-7}
150	1.20×10^7	–	–	0.6	1.50×10^{-6}	4.45×10^{-6}
200	5.28×10^5	2.25×10^5	–	0.5	3.4×10^{-5}	3.0×10^{-5}
250	4.66×10^4	1.96×10^4	–	0.49	3.8×10^{-4}	1.2×10^{-4}
300	1.37×10^4	856.6	884.4	0.48	1.3×10^{-3}	2.0×10^{-3}
350	580.3	380.7	528.9	0.47	3.1×10^{-2}	1.2×10^{-2}
400	373.4	87.28	13.87	0.46	4.8×10^{-2}	3.0×10^{-2}

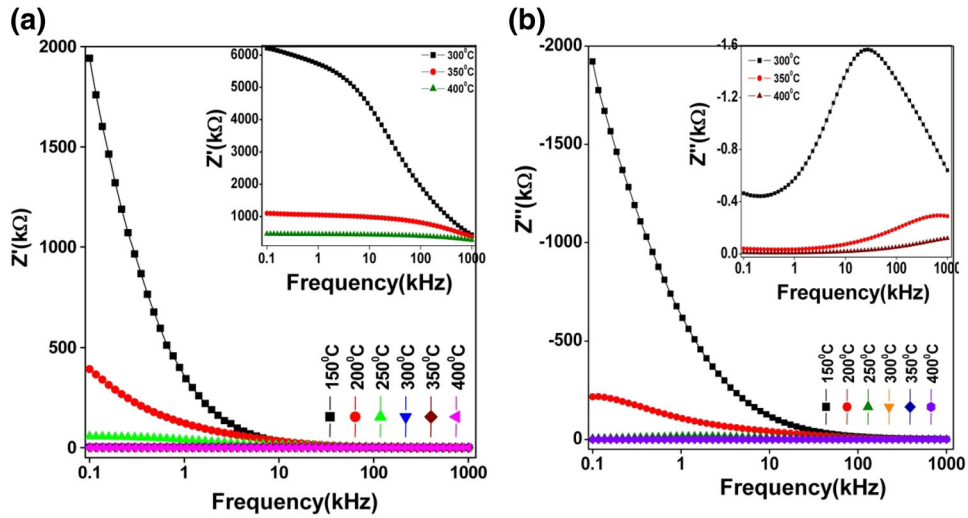

Fig. 6. Variation of (a) Z′ with frequency, (b) Z″ with frequency of $La_{0.5}K_{0.5}Ga_{0.5}V_{0.5}O_3$ at different temperatures.

The frequency dependence of Z'' at some selected temperatures is shown in Fig. 6b. This plot is suitable for evaluation of the relaxation frequency of the most resistive contribution. The absence of peaks (up to a temperature of 300°C) in the plot suggests the absence of current dissipation in this temperature region within a frequency range of 1 kHz–1 MHz. The low-temperature peaks

(<300°C) were expected to be beyond the range of frequency used. Again, in LKGVO, there may be the presence of an electrical relaxation process with the temperature dependence of the relaxation time, because with an increase in temperature, the asymmetrically broadened peaks are shifting toward the higher frequency side.[40]

Electrical Conductivity Analysis

Figure 7a shows the variation of the ac conductivity (σ_{ac}) of LKGVO with frequencies. The value of ac conductivity was calculated from the dielectric data using the relation: $\sigma_{ac} = \omega\varepsilon_r\varepsilon_0\tan\delta$, where ω is the angular frequency, ε_r is the relative dielectric constant, ε_0 is the permittivity of free space and $\tan\delta$ is the tangent loss. The nonlinear response of conductance to the application of frequency can be clearly seen (Fig. 7). The conductance remains constant for a lower frequency and then starts increasing with the increase in frequency. This value of frequency up to which the ac conductivity is constant is known as hopping frequency and, on increasing temperature, it shifts towards the higher frequency. The part below the hopping frequency corresponds to the σ_{dc}. These features suggest that the mechanism of electrical conduction in the material is a hopping type, which follows the Jonscher's power equation.

$$\sigma_{ac}(\omega) = \sigma(0) + \sigma_1(\omega) = \sigma_{dc} + A\omega^n \qquad (6)$$

where σ_{dc} is the dc conductivity at a particular temperature, A is a temperature-dependent constant, which determines the strength of polarizibility, and n is a temperature-dependent exponent in the range of $0 < n < 1$. According to many body interaction models,[43] the value of n characterizes the interaction between all dipoles participating in the polarization process. $n = 1$ implies a pure Debye case. The value of n (as given in Table I) is observed to be less than one in the studied compound, indicating the existence of a non-Debye type of conduction mechanism. From the nonlinear fitting, it is found that that the motion of the charge carriers is translational as $n < 1$. From Table I, it can be seen that the value of n decreases with increasing temperature, so our experimental results are consistent with the model based on classical hopping of electrons over a barrier,[44] which predicts the decrease in the value of n with an increase in temperature. Thus, again, it indicates that the classical concept of hopping of electrons may dominate in the system. This indicates that the conduction process is a thermally activated process.

Figure 7b shows the variation of ac conductivity (σ_{ac}) of LKGVO with the inverse of absolute temperature ($10^3/T$) at different frequencies. From the plot, the frequency-independent ac conductivity has been obtained at high temperatures, which indicates the existence of long-range movement of mobile charge carriers. The nature of variation of σ_{ac} is almost linear over a wide temperature region, obeying the Arrhenius relationship:

$$\sigma_{dc} = \sigma_0 \exp(-E_a/K_BT) \qquad (7)$$

where K_B is the Boltzmann constant, σ_0 is the pre-exponential factor, and E_a is the activation energy of the mobile charge carriers. The nature of variation of conductivity shows the NTCR behaviour of LKGVO. The calculated activation energy (E_a) of the sample in the high-temperature range at frequencies 1 kHz, 10 kHz, 100 kHz, 500 kHz and 1000 kHz is 0.82 eV, 0.71 eV, 0.59 eV, 0.51 eV and 0.46 eV, respectively, which shows the decrease in the value of activation energy of the compound with increasing frequency. The activation energies are the sum of the energies required for generation of charge carriers and their motion into the vacancies, but in case of polycrystalline materials, the defects may provide additional acceptor centers at higher temperatures.[45] Thus, on increasing the frequency, the activation energy decreases by reducing their role as an acceptor.

The Arrhenius plot for the dc electrical conductivity (σ_{DC}) of the sample is shown in Fig. 8a. The values of σ_{DC} with bulk contributions were calculated using the relation $\sigma_{DC} = R_bA/t$, where R_b is the bulk resistance, t is the thickness and A is the area of the electrode deposited on the sample. From the plot, it is observed that $\log\sigma_{DC}$ of the sample increases with increasing temperature, indicating a typical characteristic of a semiconductor (i.e., negative temperature coefficient of resistance). The change in conductivity is a thermally activated process governed by the Arrhenius relation $\sigma_{DC} = \sigma_0$ Exp $(-E_a/kT)$, where σ_0 is the pre-exponential factor, E_a is activation energy, k is the Boltzmann constant and T is absolute temperature. The increase in conductivity of the bulk with temperature may be due to the oxygen vacancies, which are usually created during high-temperature sintering, and the charge compensation.[44] The activation energy for grain conductivity was calculated from the slope of the linear portion of the plot, and was found to be 0.93 eV and 1.13 eV for low- and high-temperature regions, respectively. The conduction in the low-temperature region is, presumably, dominated by the extrinsic impurity conduction, whereas the conduction at high temperatures is due to the intrinsic defects.[46]

Figure 8b shows a typical variation of the relaxation time with the inverse of absolute temperature ($10^3/T$). The activation energy (E_a) was evaluated from the slope of the graph using the Arrhenius expression:

$$\tau = \tau_0 \mathrm{Exp}(-E_a/kT) \qquad (8)$$

where τ_0 is the pre-exponential factor, k is the Boltzmann constant and T is the absolute temperature.

From the plot, the value of activation energy is found to be 1.07 eV, which is approximately the

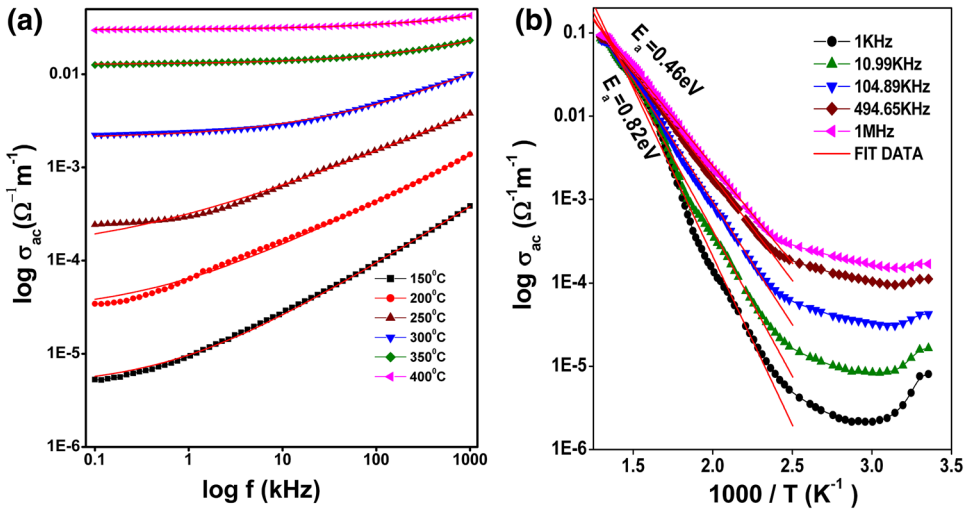

Fig. 7. Variation of ac conductivity of $La_{0.5}K_{0.5}Ga_{0.5}V_{0.5}O_3$ (a) with frequency at different temperatures and (b) with the inverse of the absolute temperature at different frequencies.

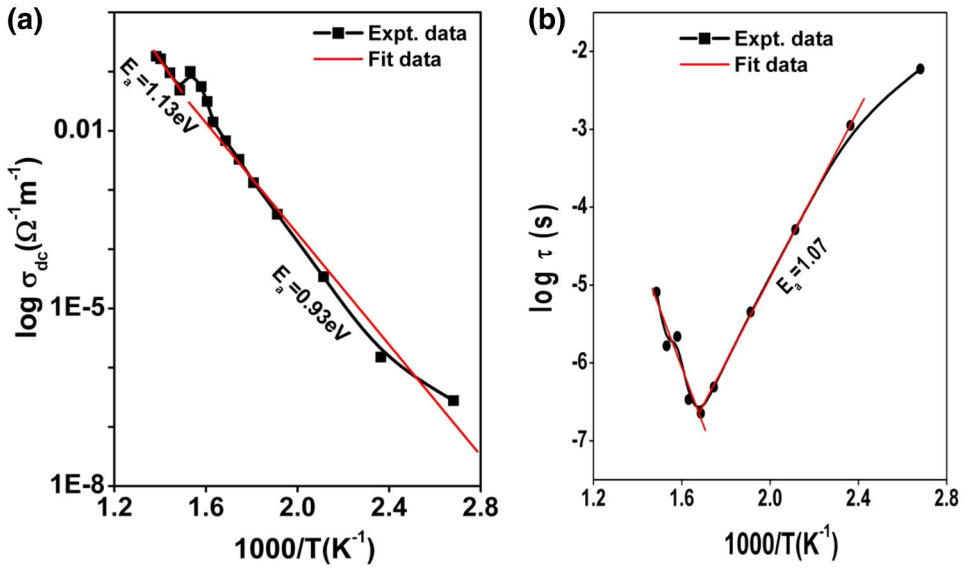

Fig. 8. Variation of (a) dc conductivity and (b) relaxation time with inverse of absolute temperature of $La_{0.5}K_{0.5}Ga_{0.5}V_{0.5}O_3$.

same as the energy required (1 eV) for motion of oxygen vacancies.[47] This confirms that the movement of oxygen vacancies is mainly responsible for the observed conductivity in the material.[47]

Leakage Current Characteristics

Figure 9b shows the current density (J) versus electric field (E) plot of LKGVO. The current density is low in the low-electric field region which increases sharply above 100 kV/cm. The abrupt increase of leakage current with an increase in electric field indicates that there may be some other conduction mechanism dominating in the conduction process.[45] The oxygen vacancies, electron transfer between Ga^{3+} to Ga^{2+}, and various defects such as stoichiometry, pores or cracks are mainly responsible for the large leakage current of the material.[46] The leakage current mechanism was analyzed using the logarithmic plot of J versus E of LKGVO. In the low-electric field region, the conduction properties follow Ohm's law, $J \propto E^{\alpha}$ where α the nonlinearity coefficient and is defined as $\alpha = d(\log J)/d(\log E)$. The leakage current density for Ohmic conduction can be expressed by $J = e\mu N_e E$, where e is the electron charge, μ is the free carrier mobility, N_e is the density of the thermally stimulate electrons, and E is the applied electric field. On increasing the applied electric field, the value of the slope (α) was observed between 1 and 2, which indicates a change of the conduction mechanism from Ohmic to a trap-free type, which is in accordance with space charge-

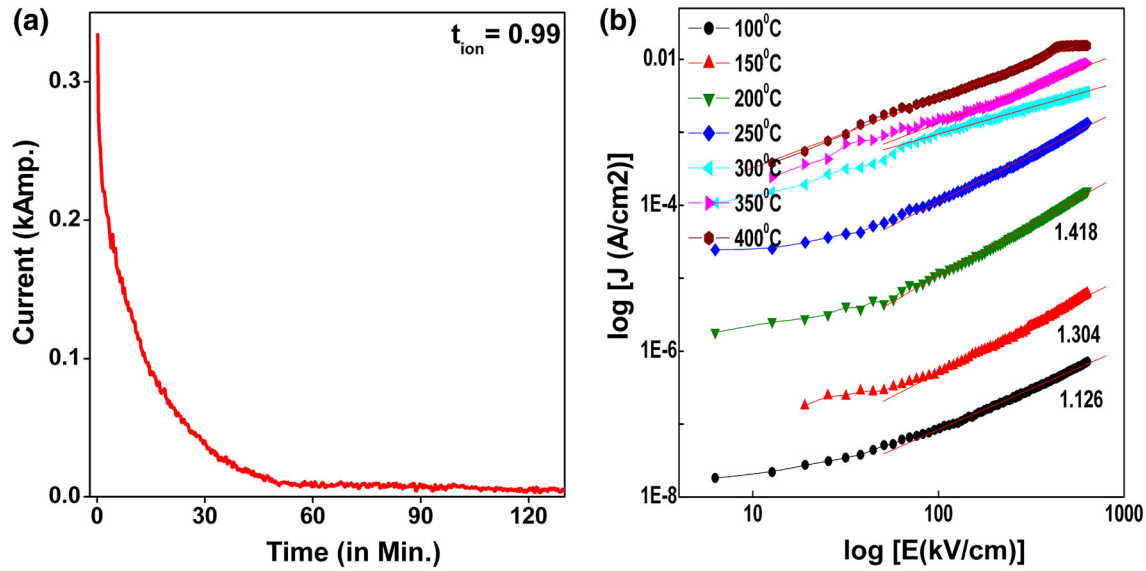

Fig. 9. Variation of (a) polarisation current as a function of time at room temperature and (b) variation of current density with electric field at various temperatures.

limited current conduction (SCLC).[48] In the high-electric field region, the density of free electrons (due to injection of charge carriers) becomes greater than the density of thermally stimulated electrons. The current density for SCLC conduction is given by

$$J = \frac{9\varepsilon_0\varepsilon_r\mu\theta}{8}\frac{V^2}{d^3} \quad (9)$$

where V is the applied voltage, ε_r is the dielectric constant, ε_0 is the permittivity of free space, d is the thickness of the sample, and h is the ratio of the total density of free electrons to the trapped electrons. The SCLC is considered normal leakage behavior and correlates with oxygen vacancies in the material.[49] Thus, the leakage current observed in LKGVO was originated from Ohmic and SCLC conduction mechanisms.

Ion Transport Number Determination

The ionic transport number of LKGVO has been obtained by using a dc polarization technique with a fixed applied voltage (400 V) across the sample cells. The variation in the polarisation current as a function of time at a fixed dc field is shown in Fig. 9a. As shown in the figure, current decreases exponentially with time. The current decreases from a maximum value with time due to polarisation of charges at respective electrodes, and, finally, it reaches a residual constant value. The initial total current (I_t) is due to ionic and electronic conduction while the constant residual current (I_e) is due to the electronic conduction only. The ionic transport number is calculated by using the equation

$$t_{\text{ion}} = 1 - \frac{\sigma_e}{\sigma_t} = 1 - \frac{I_e}{I_t} \quad (10)$$

Ideally, for pure ionic conductors, $t_{\text{ion}} = 1$ and for mixed conducting systems (partly ionic and partly electronic), it lies between zero and one. The transport number of LKGVO, as calculated from the plot (Fig. 9a) at room temperature, is found out to be 0.99. Thus, the sample behaves more as an ionic conductor than an electronic conductor at room temperature. As the value of total conductivity at room temperature is calculated to be 2.71601E−8 S/cm, the value of ionic conductivity at room temperature will be 2.69E–8 S/cm. As the ionic conductivity increases with rising temperature, the total conductivity of the sample at 400°C is found to be 4.8×10^{-2} S/cm (Table I). Therefore, we expect that the ionic conductivity of LKGVO at 400°C will also be of the order of 10^{-2} S/cm. The materials to be used in SOFCs as electrolytes should have ionic conductivity greater than or equal to 10^{-2} S/cm. Thus, we envisage that LKGVO can be used in SOFCs as an electrolyte at high temperature (≥400°C).

CONCLUSION

The polycrystalline LKGVO was prepared by using a high-temperature solid-state reaction method. The structure is confirmed to be orthorhombic. Dielectric studies showed two dielectric anomalies, suggesting the existence of some phase transitions in the material. The frequency-

temperature dependence of dielectric maximum suggests the relaxor nature of the LKGVO ceramics. The nature of variation of dielectric characteristics has been explained by the Maxwell–Wagner and Koop's phenomenological models. The unsaturated lossy hysteresis loop confirms the existence of ferroelectricity in the ionic conductor. Impedance studies reveal that material has a non-Debye type of dielectric relaxation. The grain and grain boundary effects were found to dominate at low temperatures, whereas interfacial polarization played an important role in the conduction mechanism at high temperatures. It witnesses the inter-competition between the grain boundary and electrode effect within frequency windows. It also reveals that both grain and grain boundary resistance decrease with a rise in temperature, indicating the existence of the negative temperature coefficient of resistance (NTCR) behavior of the sample. Detailed studies of electrical conductivity indicate that electrical conduction in the material is due to a thermally activated process. The temperature dependence of electrical conductivity also suggests a typical NTCR behavior for LKGVO. This may be attributed to the mobility of oxygen vacancies/defects created at elevated temperatures. The ac conductivity spectrum is found to obey Jonscher's universal power law. The dc conductivity of LKGVO was calculated to be of the order of 10^{-2} S/cm at 400°C. As LKGVO shows a high transport number and, hence, high ionic conductivity, and also exhibits stability at high temperature, the material may thus be used as an electrolyte material for SOFCs.

ACKNOWLEDGMENT

The authors are grateful to Dr. Makhanlal Nanda Goswami of Midnapore College, Medinipur, and Dr. Muhammad Shahid Anwar of IMMT, Bhubaneswar for their kind help in some of the experimental work.

REFERENCES

1. E. Iguchi, Y. Hashimoto, M. Kurumada, and F. Munakata, *J. Appl. Phys.* 94, 1758 (2003).
2. R.L. Sandstrom, E.A. Giess, W.J. Gallagher, A. Segmüller, E.I. Cooper, M.F. Chisholm, A. Gupta, S. Shinde, and R.B. Laibowitz, *Appl. Phys. Lett.* 53, 1874 (1988).
3. D.C. Dube, H.J. Scheel, I. Reaney, M. Daglish, and N. Setter, *J. Appl. Phys.* 75, 4126 (1994).
4. K. Moria, K. Shibata, H. Sagehashi, T. Ishigaki, A. Hoshikawa, S. Harjo, T. Kamiyama, K. Itoh, and T. Fukunaga, *Phys. B* 350, 1031–1034 (2004).
5. T. Ishihara, H. Matsuda, and Y. Takiya, *Solid State Ion.* 79, 147 (1995).
6. K. Kurodaa, I. Hashimoto, K. Adachi, J. Akikusa, Y. Tamou, N. Komada, T. Ishihara, and Y. Takita, *Solid State Ion.* 132, 199–208 (2000).
7. M. Kajitania, M. Matsudaa, A. Hoshikawab, S. Harjob, T. Kamiyamac, T. Ishigakib, F. Izumid, and M. Miyakea, *J. Phys. Chem. Solids* 68, 758–764 (2007).
8. Raghvendra, R.K. Singh, and P. Singh, *AIP Conf. Proc.* 1512, 976 (2013). doi:10.1063/1.4791368.
9. C. Zhang, C.-J. Li, G. Zhang, X.-J. Ning, C.-X. Li, H. Liao, and C. Coddet, *Mater. Sci. Eng., B* 137, 24–30 (2007).
10. POWDMULT, An Interactive powder diffraction data interpretation and indexing program Version 2.1, E. Wu, School of Physical Sciences, Flinders University of South Australia, Bradford Park.
11. H.P. Klung and L.B. Alexander, *X-ray Diffraction Procedure* (New York: Wiley, 1974), pp. 687–689.
12. K. Sambasiva Rao, B. Tilak, K. Ch. Varada Rajulu, A. Swathi, and H. Workineh, *J. Alloy. Compd.* 509, 7121–7129 (2011).
13. P. Petkov, D. Tsiulyanu, W. Kulisch, and C. Popov, *Nanoscience Advances in CBRN Agents Detection, Information and Energy Security*, ed. by P. Petkov, D. Tsiulyanu, W. Kulisch, and C. Popov (Springer, 2015).
14. L.M. El Nadi, Modern Trends in Physics Research—Third International Conference on Modern, Egypt, 6–10 April 2008.
15. J. Yang, Y. Zhao, and R.L. Frost, *Spectrochim. Acta Part A* 74, 398–403 (2009).
16. A.C. Tas, P.J. Majewski, and F. Aldinger, *J. Am. Ceram. Soc.* 85, 1420 (2002).
17. S. Mandal, S. Hazra, D. Das, and A. Ghosh, *J. Non Cryst. Solids* 183, 315–319 (1995).
18. D.L. Wood and J. Tauc, *Phys. Rev. B* 5, 3144–3152 (1972).
19. V.S. Marques, L.S. Cavalcante, J.C. Sczancoski, E.C. Paris, J.M.C. Teixeira, J.A. Varela, F.S. De Vicente, M.R. Joya, P.S. Pizani, M. SiuLi, M.R.M.C. Santos, and E. Longo, *Spectrochim. Acta Part A* 74, 1050–1059 (2009).
20. K.E. Babu, N. Murali, K.V. Babu, P.T. Shibeshi, and V. Veeraiah, *AIP Conf. Proc.* 1620, 173 (2014). doi:10.1063/1.4898236.
21. A. Rebola, D.D. Fong, J.A. Eastman, S. Öğut, and P. Zapol, *Phys. Rev. B* 87, 245117 (2013).
22. M.J. Weber, *Handbook of Optical Materials* (Boca Raton: CRC Press, 2003).
23. C.G. Koops, *Phys. Rev.* 83, 121–124 (1951).
24. B.N. Parida and P.R. Das, *J. Alloys Compd.* 585, 234–239 (2014).
25. S. Chandarak, A. Ngamjarurojana, S. Srilomsak, P. Laoratanakul, S. Rujirawat, and R. Yimnirun, *Ferroelectrics* 410, 75–81 (2011).
26. H. Mahamoud, B. Louati, F. Hlel, and K. Guidara, *J. Alloys Compd.* 509, 6083–6089 (2011).
27. D.C. Dube, H.J. Scheel, I. Reaney, M. Daglish, and N. Setter, *J. Appl. Phys.* 75, 4126 (1994). doi:10.1063/1.355993.
28. T.A. Patil, V.M. Jamadar, and S.H. Chavan, *Bull. Mater. Sci.* 9, 331–336 (1987).
29. P.R. Das, L. Biswal, B. Behera, and R.N.P. Choudhary, *Mater. Res. Bull.* 44, 1214 (2009).
30. S.M. Pilgrim, A.E. Sutherland, and S.R. Winzer, *J. Am. Ceram. Soc.* 73, 3122 (1990).
31. F.A. Kröger and H.J. Vink, *Solid State Phys.* 3, 307 (1956).
32. V. Raghavan, *Material Science and Engineering* (New Delhi: Prentice-Hall of India, 2004).
33. M. Li, M.J. Pietrowski, R.A. De Souza, H. Zhang, I.M. Reaney, S.N. Cook, J.A. Kilner, and D.C. Sinclair, *Nat. Mater.* 13, 31–35 (2014).
34. Z.G. Yi, Y.X. Li, Z.Y. Wen, S.R. Wang, J.T. Zeng, and Q.R. Yin, *Appl. Phys. Lett.* 86, 192906 (2005).
35. B.I. Lazoryak, O.V. Baryshnikova, S. Yu. Stefanovich, A.P. Malakho, V.A. Morozov, A.A. Belik, I.A. Leonidov, O.N. Leonidov, and G. Van Tendelooo, *Chem. Mater.* 15, 3003–3010 (2003).
36. D. Ming, J.M. Reau, and J. Ravez, *Ferroelectrics* 196, 147–150 (1997).
37. V. Andriamampianina, J. Ravez, D. Ming, and J.M. Reau, *Ferroelectrics* 195, 39–42 (1997).
38. V. Hornebecq, J.-M. Reau, A. Villesuzanne, C. Elissalde, and J. Ravez, *J. Mater. Chem.* 8, 2423–2428 (1998).
39. M.A.L. Nobre and S. Lanfredi, *J. Phys. Chem. Solids* 64, 2457 (2003).
40. M. Ram, *J. Alloy. Compd.* 509, 1744–1748 (2011).
41. J.R. MacDonald, *Impedance Spectroscopy: Emphasizing Solid Materials and Systems* (New York: Wiley, 1987).
42. T. Acharya and R.N.P. Choudhary, *J. Electron. Mater.* 44, 271–280 (2015).
43. J.K. Lee, H.W. Park, H.W. Choi, J.E. Kim, S.J. Kim, and Y.S. Yang, *J. Korean Phys. Soc.* 47, 267–270 (2005).

44. K. Lily, K. Kumari, and R.N.P. Prasad, Choudhary. *J. Alloy. Compd.* 453, 325–331 (2008).
45. C. Karthik and K.B.R. Varma, *J. Phys. Chem. Solids* 67, 2437 (2006).
46. E. Venkata Ramana, M.P.F. Graça, M.A. Valente, and T. Bhima Sankaram, *J. Alloys Compd.* 583, 198–205 (2014).
47. W.D. Kingery, H.K. Browen, and D.R. Ulhman, *Introduction to Ceramics* (New York: Wiley, 1976), pp. 516–532.
48. N. Zidi, A. Chaouchi, S. d'Astorg, M. Rguiti, and C. Courtois, *J. Alloys Compd.* 590, 557–564 (2014).
49. S. Dash, R.N.P. Choudhary, R.D. Piyush, and A. Kumar, *Appl. Phys. A* 118, 1023–1031 (2015).